Wave Motion 113 (2022) 102966

Contents lists available at ScienceDirect

Wave Motion

journal homepage: www.elsevier.com/locate/wamot

Navigating the Hilbert space of elastic bell states in driven coupled waveguides

M. Arif Hasan [a,*], Trevor Lata [b], Pierre Lucas [b], Keith Runge [b], Pierre A. Deymier [b]

[a] Department of Mechanical Engineering, Wayne State University, Detroit, MI 48202, USA
[b] Department of Materials Science and Engineering, The University of Arizona, Tucson, AZ 85721, USA

ARTICLE INFO

Article history:
Received 26 August 2020
Received in revised form 19 April 2022
Accepted 11 May 2022
Available online 30 May 2022

Keywords:
Elastic waves
Acoustic waveguides
Nonseparability
Superpositions of states

ABSTRACT

Externally driven arrays of coupled elastic waveguides have been shown to support nonseparable elastic superpositions of states that are analogous to entangled Bell states in a multipartite quantum system. Here, the "subsystems" correspond to spatial eigen modes characterized by the amplitude and phase difference between the waveguides. We show experimentally that the driving frequency, the relative amplitudes, and phases of the drivers applied to the waveguides, are critical parameters for exploring the elastic Bell states' Hilbert space. We also demonstrate experimentally the capability of tuning the degree of nonseparability of the superpositions of elastic states. The degree of nonseparability is quantified by calculating the entropy of entanglement. Finally, in support of the experimental observations, we show theoretically that nonlinearity in the elastic behavior of the coupling medium (epoxy) and heterogeneities in the coupling along the waveguides can serve as design parameters in extending the range of the elastic Bell states' Hilbert space that can be explored.

1. Introduction

Quantum entanglement, the nonclassical correlation between quantum systems, is an essential ingredient for applications in quantum information science [1]. One of the properties of quantum entangled states is nonseparability, which is however not limited to quantum systems. Nonseparable states of classical waves [2] are sometimes referred to as classically or nonquantum entangled [2–14]. While such classical nonseparable waves do not exhibit the uniquely quantum property of nonlocality, they manifest all other properties of locally entangled states [15], such as nonseparable linear combinations of tensor product states between different degrees of freedom of the same physical manifestation similar to the degree of freedom of a single quantum particle [16]. They have found applications in quantum information science [4,17,18] and metrology [4,19]. Another rather important application is in quantum computing since quantum computing harnesses the nonseparability of entangled states [20]. To date, the study of local nonseparable superpositions of states has essentially focused on the area of optics [7,19,21–30], and much less attention has been paid to other classical waves such as elastic waves; yet, remarkable quantum analogous behaviors of sound are emerging, such as the notions of elastic pseudospin [31–33] and Zak/Berry phase [34–36]. Recently, we have shown that parallel arrays of one-dimensional (1D) elastic waveguides composed of aluminum rods that are coupled along their length with epoxy and are driven externally, can capture the characteristic of nonseparability (classical entanglement) between different degrees

* Corresponding author.
E-mail addresses: hasan.arif@wayne.edu (M.A. Hasan), tlata157@email.arizona.edu (T. Lata), pierre@arizona.edu (P. Lucas), krunge@bellsouth.net (K. Runge), deymier@arizona.edu (P.A. Deymier).

https://doi.org/10.1016/j.wavemoti.2022.102966
0165-2125/

of freedom of the same physical manifestation [12–14]. These nonseparable superpositions of elastic states, analogous to Bell states, are constructed as a superposition of elastic waves, each a product of a spatial eigen mode part and a plane wave. The plane wave part describes the elastic wave along the length of the waveguides and the spatial eigen modes characterize the amplitude and phase difference between waveguides i.e., across the array of waveguides. These states lie in the tensor product Hilbert space of the two-dimensional subspaces associated with the degrees of freedom along and across the waveguide array. Experimentally we demonstrated that the amplitude coefficients of these nonseparable states are complex due to the dissipative nature of the coupling medium. Navigating portions of the elastic Bell states' Hilbert space necessitated means of tuning these complex amplitudes [12–14]. In the area of optics, the generation of Bell states and the tuning of their amplitudes is well established [37–41]. In optics, the phase of the entangled states are commonly used to create a wide range of quantum states with controllable degrees of entanglement [40,42]. The phase of the entangled states are selected by changing the half-wave plate and quarter-wave plate orientation [40,42]. However, to the best of our knowledge, no similar work has been done in elastic systems. It is the objective of the present study to experimentally demonstrate the possibility of not only generating elastic Bell states but also tuning their amplitude over a broad region of the Bell states' Hilbert space. More specifically, we show experimentally that the frequency, relative amplitudes and phases of the external drivers applied to the waveguides, are critical parameters for navigating the elastic Bell states' Hilbert space. To explain the experimental observations, we have developed a theoretical model, which in addition to dissipation, accounts for the weak elastic nonlinearity of the medium (epoxy) coupling the essentially linear waveguides, as well as for heterogeneities in the coupling medium along the waveguides. Nonlinear elasticity and heterogeneity of the coupling medium are shown to be potential design parameters in extending the range of the elastic Bell states' Hilbert space that can be explored via the external drivers.

2. Background

We briefly review the theory behind the behavior of nonseparable elastic states in parallel arrays of coupled 1D elastic waveguides. The experimental realization of nonseparable superposition of elastic states requires a mechanical system in which elastic wave behavior is effectively described by:

$$\left\{H.I_{N\times N} + k_c^2 M_{N\times N}\right\} U_N = 0, \tag{1}$$

where $H\left(=\frac{\partial^2}{\partial t^2} - \beta^2 \frac{\partial^2}{\partial x^2}\right)$ is the dynamical differential operator that models the propagation of elastic waves along the waveguides (in $x-$direction) and β is proportional to sound speed in the waveguides. In Eq. (1), k_c is the coupling stiffness between the waveguides, U_N is a vector and $U_i, i = 1, 2, \ldots, N$, represent the displacement of the ith waveguide. $I_{N\times N}$ is the $N \times N$ identity matrix and the coupling matrix operator $M_{N\times N}$ describes the elastic coupling between waveguides. The experimental system can be modeled as $N = 3$ mass and spring chains that are elastically coupled with a total of N_m identical masses in each chain. The discrete elastic equations of motion are then given by:

$$\begin{aligned} m\ddot{u}_n - k_{nn}\left(u_{n+1} - 2u_n + u_{n-1}\right) - k_{c'}\left(v_n - u_n\right) &= 0,\\ m\ddot{v}_n - k_{nn}\left(v_{n+1} - 2v_n + v_{n-1}\right) - k_{c'}\left(u_n - v_n\right) - k_c\left(w_n - v_n\right) &= 0,\\ m\ddot{w}_n - k_{nn}\left(w_{n+1} - 2w_n + w_{n-1}\right) - k_{c'}\left(v_n - w_n\right) &= 0, \end{aligned}$$

In the above equation, u_n, v_n, andw_n are the displacements of nth mass of chain 1, 2, and 3, respectively, and $n = 2, \ldots, N_m - 1$. The term k_{nn} describes the coupling constant of the nearest-neighbor interaction, $k_{c'}$ describes the stiffness of the springs that couples the chains, and m is the mass. In the limit of long wavelength compared to the inter-mass spacing a, the equations of motion of the three coupled linear harmonic chains of masses and springs become:

$$\begin{aligned} \frac{\partial^2 u}{\partial t^2} - \beta^2 \frac{\partial^2 u}{\partial x^2} - k_c^2\left(v - u\right) &= 0,\\ \frac{\partial^2 v}{\partial t^2} - \beta^2 \frac{\partial^2 v}{\partial x^2} - k_c^2\left(u - v\right) - \alpha^2\left(w - v\right) &= 0,\\ \frac{\partial^2 w}{\partial t^2} - \beta^2 \frac{\partial^2 w}{\partial x^2} - k_c^2\left(v - w\right) &= 0, \end{aligned}$$

where $\beta^2 = k_{nn}a^2/m$ and $k_c^2 = k_{c'}/m$. In a simple form:

$$\left(\frac{\partial^2}{\partial t^2} - \beta^2 \frac{\partial^2}{\partial x^2}\right).\begin{pmatrix} 1 & 0 & 0\\ 0 & 1 & 0\\ 0 & 0 & 1 \end{pmatrix}\begin{pmatrix} u\\ v\\ w \end{pmatrix} + k_c^2\begin{pmatrix} 1 & -1 & 0\\ -1 & 2 & -1\\ 0 & -1 & 1 \end{pmatrix}\begin{pmatrix} u\\ v\\ w \end{pmatrix} = 0.$$

By comparing the above equation with Eq. (1), we obtain the coupling matrix as

$$M_{3\times 3} = \begin{pmatrix} 1 & -1 & 0\\ -1 & 2 & -1\\ 0 & -1 & 1 \end{pmatrix}.$$

Therefore, for the case of three coupled waveguides ($N = 3$), the coupling matrix takes the form $M_{3\times3} = \begin{pmatrix} 1 & -1 & 0 \\ -1 & 2 & -1 \\ 0 & -1 & 1 \end{pmatrix}$ and the three spatial eigen vectors corresponding to the eigen values $\lambda_1 = 0$, $\lambda_1 = 1$, and $\lambda_3 = 3$, are: $E_1 = \frac{1}{\sqrt{3}}\begin{pmatrix} 1 \\ 1 \\ 1 \end{pmatrix}, E_2 = \frac{1}{\sqrt{2}}\begin{pmatrix} 1 \\ 0 \\ -1 \end{pmatrix}, E_3 = \frac{1}{\sqrt{6}}\begin{pmatrix} 1 \\ -2 \\ 1 \end{pmatrix}$ [13]. E_1 corresponds to a linear band passing through the origin of wave numbers, E_2 and E_3 correspond to two parabolic bands with non-zero spatial eigen values [12,43,44]. The spatial modes represent the displacement across the array of waveguides. In addition, the plane waves degrees of freedom along the waveguides can be represented by e^{ikx}, where k is a wave number. Solution to Eq. (1) are therefore product of a plane wave part and a spatial eigen mode. Subsequently, since Eq. (1) is linear, it supports superposition of elastic states, each a product of a plane wave part and a spatial eigen mode. By selecting plane wave parts with different wave numbers and different spatial eigen modes, these superpositions of elastic waves can be chosen to be non-factorizable i.e., they cannot be written as a single product of a plane wave and a spatial mode. These acoustic nonseparable superpositions are analogous to Bell states [12–14].

2.1. Creation of a nonseparable Bell state

By driving the array of coupled waveguides with an external driver, $\vec{F}e^{i\omega t}$, where the components of the vector $\vec{F}$ represent the driving force acting on each waveguide and ω is the driving frequency, one can excite a nonseparable superposition of states whose characteristics are given by

$$U_N(t) = \left(\sum_{k'} A_1E_1e^{ik'x} + \sum_{k''} A_2E_2e^{ik''x} + \sum_{k'''} A_3E_3e^{ik'''x}\right)e^{i\omega t}. \tag{2}$$

Except for special choices of A_1, A_2, and A_3, the above superposition cannot be factored as a single product, and thus is nonseparable. The k', k'', k''' are the wavenumbers associated with the dispersion relations of each spatial eigen mode E_1, E_2, E_3. In Eq. (2) a discrete summation is used over the wave numbers, since in the case of a finite number of finite length waveguides, the plane wave and spatial parts are both discrete. The Bell state coefficients A_i; $i = 1, 2, 3$ are complex amplitudes [12]

$$A_i(k) = \frac{E_i.\vec{F}}{\omega_{0,i}^2(k) - \omega^2 - i\eta\omega},$$

where $\omega_{0,i}$; $i = 1, 2, 3$ are the eigen frequencies corresponding to the bands of the E_i spatial mode eigen vectors and η is the viscous damping coefficient that models the experimental dissipation. We would like to note that though the dissipation term appears on the right side of Eq. (2), to theoretically calculate the eigenvectors (E_i; $i = 1, 2, 3$) we have used a conservative system (Eq. (1)). As a result, we assume that the coupled waveguides experimental eigenmodes are close to the eigenvectors obtained from (1) using the eigenmode analysis. We also note from Eq. (2) that at steady state, the displacement field, U_N, takes the form of a linear combination of all frequency modes [13,45]. However, by exploiting the orthogonality of E_1, E_2 and E_3, one may employ a driving force that can select specific spatial eigen modes or linear combinations of spatial modes. For instance, a linear combination of E_2 and E_3 such that $\vec{F} = (1-\alpha)E_2 + \alpha E_3$, with the parameter α, controls the contribution of the two linear combinations of spatial eigen modes E_2 and E_3. For $\alpha = 0$, the input driving force $\vec{F} = E_2$, will excite a pure E_2 spatial mode, and for $\alpha = 1$, a pure E_3 mode. For all other α values, the state is a nonseparable superpositions of E_2 and E_3.

In addition to the particular driving force $\vec{F}$ that may be a linear combination of E_2 and E_3, and since the complex amplitudes $A_i(k)$ may have narrow bandwidths, it is also possible to choose a particular isofrequency state ω_I that will limit the excitation, predominantly, to a single plane wave state in the bands of the E_2 and E_3 modes, i.e., k_2 for E_2 spatial mode band and k_3 for E_3 spatial mode band [12,43,44]. In this case, Eq. (2) reduces to,

$$U_N(t) = \left(A_1E_1e^{ik_1x} + A_2E_2e^{ik_2x} + A_3E_3e^{ik_3x}\right)e^{i\omega_I t}. \tag{3}$$

For the sake of compactness, we use the ket notation of quantum mechanics [14] to represent the plane wave and spatial modes. For this, we denote the discrete spatial states by $|E_i\rangle$ and the discrete plane wave states by $|k_i\rangle$. Eq. (3) becomes:

$$U_N(t) = \left(A_1|E_1\rangle|k_1\rangle + A_2|E_2\rangle|k_2\rangle + A_3|E_3\rangle|k_3\rangle\right)e^{i\omega_I t}. \tag{4}$$

Finally, we can also consider driving the system with more complex forms. For instance, we choose $\vec{F}e^{i\omega_I t} = \left[(1-\alpha)E_2 + e^{i\phi_0}\gamma\alpha E_3\right]e^{i\omega_I t}$. For a fixed α value i.e., for a particular nonseparable state, by tuning γ it is possible to see the effect of the nonseparable state on the strength of the input force. We have also introduced a driving phase parameter ϕ_0. This is the relative phase between the component of the driver that excites the E_2 and E_3 spatial modes. In this paper, we investigate experimentally and theoretically how the complex quantities A_i can be tuned via the control parameters $\alpha, \gamma, \phi_0,$ and ω_I.

2.2. Bell state complex coefficients

The Bell state complex coefficients can be determined by the expression [12–14]:

$$A_1 |E_1\rangle |k_1\rangle + A_2 |E_2\rangle |k_2\rangle + A_3 |E_3\rangle |k_3\rangle = \frac{A_1}{\sqrt{3}} \begin{pmatrix} 1 \\ 1 \\ 1 \end{pmatrix} |k_1\rangle + \frac{A_2}{\sqrt{2}} \begin{pmatrix} 1 \\ 0 \\ -1 \end{pmatrix} |k_2\rangle + \frac{A_3}{\sqrt{6}} \begin{pmatrix} 1 \\ -2 \\ 1 \end{pmatrix} |k_3\rangle = \begin{pmatrix} C_1 e^{i\phi_1} \\ C_2 e^{i\phi_2} \\ C_3 e^{i\phi_3} \end{pmatrix}, \quad (5)$$

where C_i; $C_1 = \max(U_1(t))$, $C_2 = \max(U_2(t))$, $C_3 = \max(U_3(t))$, are the maximum amplitudes of each waveguide and ϕ_i; $i = 1, 2, 3$ are the phases of each waveguide. Since only relative phase is meaningful, the right-hand side of Eq. (5) can be further simplified in terms of the phase differences, ϕ_{ij}; $i, j = 1, 2, 3$ and $i \neq j$, between the transmissions of each waveguide as:

$$\begin{pmatrix} C_1 \\ C_2 e^{-i\phi_{12}} \\ C_3 e^{-i\phi_{13}} \end{pmatrix}, \quad (6)$$

where $\phi_{12} = \phi_1 - \phi_2$, $\phi_{13} = \phi_1 - \phi_3$, and for the sake of simplicity we assume $\phi_1 = 0$. Using Eq. (5), we then can calculate the complex amplitudes A_i in terms of measured waveguide amplitudes and relative phases.

2.3. Entropy of "entanglement"

Let us form an orthonormal basis for the states of the coupled elastic waveguides in the form of the four tensor products: $\Phi_1 = |E_2\rangle |k_2\rangle$, $\Phi_2 = |E_2\rangle |k_3\rangle$, $\Phi_3 = |E_3\rangle |k_2\rangle$ and $\Phi_4 = |E_3\rangle |k_3\rangle$. The two vectors $|E_2\rangle$ and $|E_3\rangle$ form an orthonormal basis for a two-dimensional Hilbert space, H_E. $|k_2\rangle$ and $|k_3\rangle$ form another orthonormal basis for a two-dimensional Hilbert space, H_k. Φ_1, Φ_2, Φ_3, and Φ_4 form the basis of a four-dimensional Hilbert product space $H_{E,k} = H_E \otimes H_k$. In that basis, when the drivers are set to excite only isofrequency superpositions of only spatial eigen modes E_2 and E_3, U_N takes the nonseparable form:

$$U_N(t) = (A_2\Phi_1 + A_3\Phi_4) e^{i\omega t}. \quad (7)$$

To quantify the level of nonseparability of this superposition of states, we calculate the entropy of classical 'entanglement' [12,14,46]. The expression for the entropy of "entanglement", S, can be written as [12,14]:

$$S = -\frac{1}{|A_2|^2 + |A_3|^2} \left(A_2 A_2^* ln \frac{A_2 A_2^*}{|A_2|^2 + |A_3|^2} + A_3 A_3^* ln \frac{A_3 A_3^*}{|A_2|^2 + |A_3|^2} \right). \quad (8)$$

We note that if $A_2 = A_3$, then $S(\rho_{OAM}) = ln2$, and the state is maximally "entangled". By controlling the amplitude and phase of A_2 and A_3, one can control the degree of nonseparability of elastic Bell states.

3. Experimental results

The experimental set up is the same as that reported in Refs. [12–14]. Some details are provided in the Supplemental Material. To experimentally realize a nonseparable superpositions of E_2 and E_3 spatial modes, as shown in Eq. (4), we need to drive the coupled waveguides at isofrequency state ω_I and need to tune that state between the E_2 and E_3 pure states. We identified two isofrequency states, $\omega_I = 48.8$ kHz and $\omega_I = 60$ kHz that enable us to overlap E_2 and E_3 modes (see [12,13] and the Supplemental Material Note S1). When the system is in a pure E_2 spatial mode, the phase differences between the output transmissions for each pair of rods should be $\phi_{12}^{E_2} = \phi_{23}^{E_2} = \frac{\pi}{2}, \phi_{13}^{E_2} = \pi$, where $\phi_{ij} = \frac{180}{\pi} \cos^{-1}\left(\frac{U_i(t).U_j(t)}{|U_i(t)||U_j(t)|}\right)$ is the phase difference between rods i and j. Similarly, for a pure E_3 mode, the phase differences should be $\phi_{12}^{E_3} = \phi_{23}^{E_3} = \pi, \phi_{13}^{E_3} = 0$. From a practical point of view, pure states are an idealization; irrespective of how carefully a state is prepared, uncertainties in the experimental system and setup make it difficult to experimentally realize pure states. In our elastic system, uncertainties can arise from material impurity, nonuniformity in the epoxy coupling, lack of identical responses among different transducers, nonuniform contact pressure between the waveguides and the ultrasonic couplant. Therefore, in the experiment, to obtain an output of almost pure E_2 or E_3 spatial mode, we found that we need to use the driving forces $\vec{F} = \frac{1}{\sqrt{2.01}} \begin{pmatrix} 1 \\ -0.1 \\ -1 \end{pmatrix} = E_{2'}$ and $\vec{F} = \frac{1}{\sqrt{6.96}} \begin{pmatrix} 1 \\ -2 \\ 1.4 \end{pmatrix} = E_{3'}$, which result in the phase differences $\phi_{12}^{E_{2'}} = 0.59\pi, \phi_{23}^{E_{2'}} = 0.46\pi, \phi_{13}^{E_{2'}} = 0.95\pi$ and $\phi_{12}^{E_{3'}} = 0.99\pi, \phi_{23}^{E_{3'}} = 0.95\pi, \phi_{13}^{E_{3'}} = 0.06\pi$ (see Supplemental Material Note S2 for details). These states are the closest to pure states that we were able to achieve with our experimental setup. We note that because of the small deviation from the pure states 2 and 3, the system must also support some small contribution from the E_1 mode.

In the subsequent subsections, we will tune the system with a driving force of the form

$$\vec{F} e^{i\omega_I t} = \left[(1-\alpha) E_{2'} + e^{i\phi_0} \gamma \alpha E_{3'} \right] e^{i\omega_I t}. \quad (9)$$

We will analyze two approaches to navigate the Hilbert space of superpositions of elastic states: (i) fixed ϕ_0 but variable α and γ, and (ii) fixed α and γ but variable ϕ_0. Here, the phase ϕ_0 is introduced simply by using the signal generators.

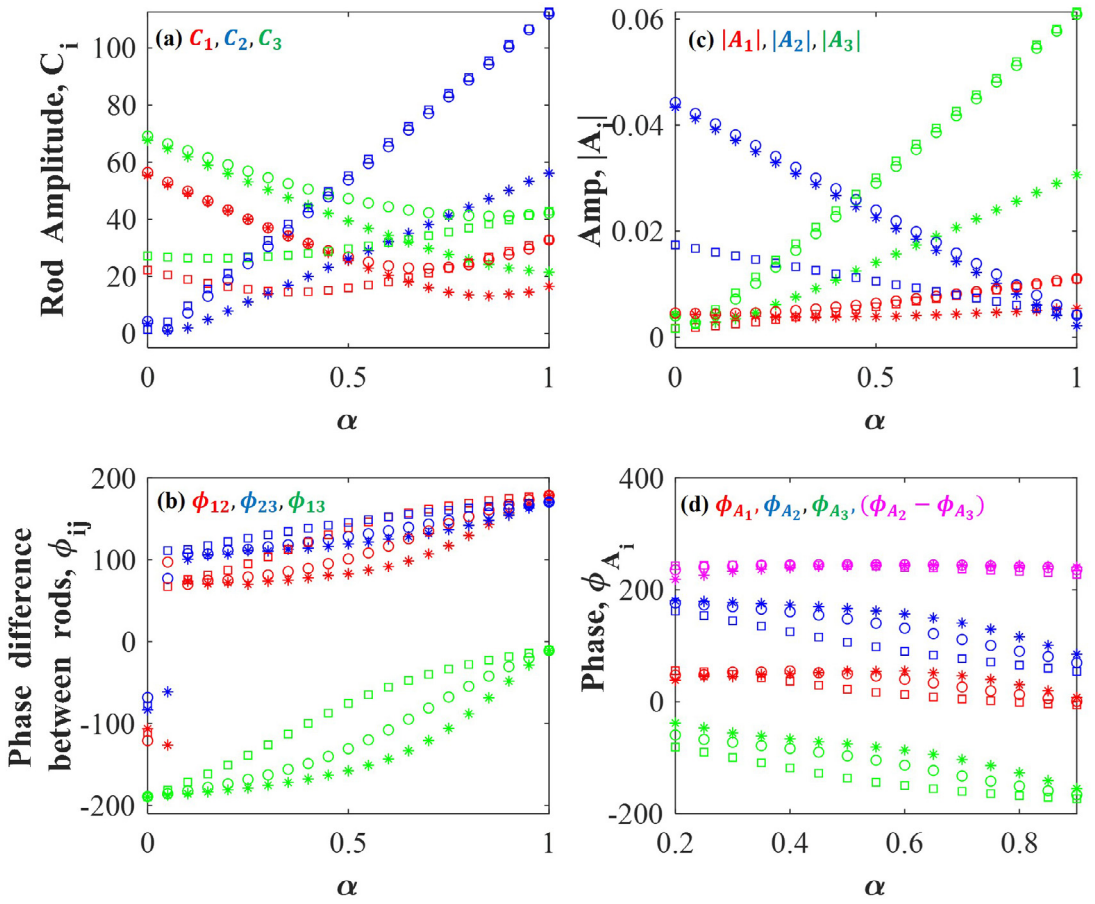

Fig. 1. Measured amplitude and phase characteristics of the elastic states in the space of rods (left panels) and calculated amplitudes and phase of states in the Hilbert space of superpositions of product states (right panels). These states are excited by the external driving force $\vec{F}e^{i\omega_l t}$; $\vec{F} = (1-\alpha)E_{2'} + e^{i\phi_0}\gamma\alpha E_{3'}$ with $\phi_0 = 0$. Dependency on α of the (**a**) maximum amplitudes of each waveguide C_i, (**b**) phase differences (ϕ_{ij}) between pairs of rods, (**c**) modulus of the complex amplitudes $|A_i|$, and (**d**) arguments ϕ_{A_i}. In the plots, asterisks correspond to $\gamma = 0.5$, circles correspond to $\gamma = 1.0$, and squares corresponds to $\gamma = 2.5$. The driving frequency $\omega_l = 48.8$ kHz. The amplitudes are in arbitrary units and the phases are in degrees. Since $(\phi_{A_2} - \phi_{A_3})$ is not well defined close to the pure spatial modes $E_{2'}$ or $E_{3'}$ (i.e., at $\alpha = 0$ amplitude $A_3 \cong 0$, and at $\alpha = 1$ amplitude $A_2 \cong 0$), graph (d) is limited to the range $\alpha = [0.2, 0.9]$.

3.1. Exploring the Hilbert space by tuning the relative driving amplitudes

We first drive the coupled waveguides at isofrequency state of $\omega_l = 48.8$ kHz for different values of α and γ, and for a fixed $\phi_0 = 0$. The amplitude and phase characteristics are reported in two spaces, namely the space of the rods (Eq. (6)) and the Hilbert space of superpositions of product states (see Eq. (7)). Fig. 1 shows the measured amplitude and phase characteristics of the elastic states at each rod. Figs. 1a and 1b show the variations of the maximum amplitudes of each waveguide C_i and the phase difference (ϕ_{ij}) between the transmissions for each pair of waveguides as functions of α. From these plots we indeed see that the parameter α can be used to tune the eigen mode superposition, since for $\alpha \neq 0$ and $\alpha \neq 1$, the output mode is a linear combinations of spatial eigen modes E_2, E_3 with corresponding k-labeled plane waves. In the plots, asterisks correspond to $\gamma = 0.5$, circles correspond to $\gamma = 1.0$, and squares correspond to $\gamma = 2.5$.

We now determine the Bell state complex coefficients for the different driving amplitudes. For the case of finite length waveguides, the wave numbers are integer multiples of $2\pi/2L$, where L is the length of the finite waveguides. Because of variabilities in the experimental system as well as the setup, we anticipate that the superposition of states that is excited may include E_1 spatial modes in addition to the desired E_2 and E_3 modes. We therefore seek superpositions in the form

$$\frac{A_{1_{k_1}}}{\sqrt{3}}\begin{pmatrix}1\\1\\1\end{pmatrix}|k_1\rangle + \frac{A_{1_{k_{1'}}}}{\sqrt{3}}\begin{pmatrix}1\\1\\1\end{pmatrix}|k_{1'}\rangle + \frac{A_2}{\sqrt{2}}\begin{pmatrix}1\\0\\-1\end{pmatrix}|k_2\rangle + \frac{A_3}{\sqrt{6}}\begin{pmatrix}1\\-2\\1\end{pmatrix}|k_3\rangle = \begin{pmatrix}C_1\\C_2e^{-i\phi_{12}}\\C_3e^{-i\phi_{13}}\end{pmatrix}. \tag{10}$$

We introduce, for the sake of completeness, two E_1 modes which wave vectors k_1 and $k_{1'}$ possess corresponding frequencies close to the driving frequency (see Supplemental Material Note S1). Hence, for the case of isofrequency state

at $\omega_I = 48.8$ kHz, we find $k_1 = \frac{2\pi}{2L}12$, $k_{1'} = \frac{2\pi}{2L}13$, $k_2 = \frac{2\pi}{2L}13$ and $k_3 = \frac{2\pi}{2L}11$ (see Supplemental Material Note S1). At $x = L$, where the measurements are performed, the plane wave terms are all equal to ± 1 and Eq. (10) reduces to:

$$\frac{A_1}{\sqrt{3}}\begin{pmatrix}1\\1\\1\end{pmatrix} + \frac{A_2}{\sqrt{2}}\begin{pmatrix}1\\0\\-1\end{pmatrix} + \frac{A_3}{\sqrt{6}}\begin{pmatrix}1\\-2\\1\end{pmatrix} = \begin{pmatrix}C_1\\C_2 e^{-i\phi_{12}}\\C_3 e^{-i\phi_{13}}\end{pmatrix}, \tag{11}$$

where $A_1 = A_{1_{k_{1'}}} - A_{1_{k_1}}$. Using Eq. (11), we calculate the complex amplitudes A_i. Fig. 1c shows the modulus of the measured complex amplitudes $|A_i|$ as a function of the driving parameter α. From Fig. 1c we observe, as anticipated, that as the superposition evolves from the E_2 pure state ($\alpha = 0$) to the E_3 pure state ($\alpha = 1$), the value of $|A_2|$ decreases and $|A_3|$ increases. Moreover, though the amplitude $|A_1|$ shows some variation with α, as expected, it remains quite small in comparison to $|A_2|$ and $|A_3|$. We also observe that the variation of $|A_1|$ is not linear, which may be the consequence of presence of nonlinearity in the experimental sample (this point will be discussed in more details below in Eqs. (13)–(14) and in the Numerical Section). The elastic state of the system is essentially a nonseparable state of the form given by Eq. (7). From Fig. 1d we see that though the absolute values of the arguments of the complex amplitudes i.e., ϕ_{A_i} varies significantly with the excitation parameter α, the relative phase between the modes 2 and 3, i.e., $\left(\phi_{A_2} - \phi_{A_3}\right)$ varies only weakly with α. From Fig. 1d we also observe that for fixed α, the relative phase between the E_2 and E_3 parts of the nonseparable superposition of states also varies weakly with γ. In summary, for fixed $\phi_0 = 0$, tuning the driving parameters αandγ leads to significant variations in the modulus of the complex amplitudes of elastic superpositions of product states but affects only weakly the phase of the nonseparable states.

We now calculate the entropy of classical 'entanglement' using Eq. (8), to quantify the level of nonseparability of the superposition of elastic states. From Fig. 1c we see that the complex coefficient A_1 is much smaller in comparison to A_2 and A_3. Hence, we have neglected the effect of A_1 in Eq. (8). We calculate the entropy of 'entanglement', S, for the nonseparable states corresponding to $\gamma = 1$ and $\alpha = 0.5$. Using the data of Fig. 1, we determine $S = 0.97ln2$. This superposition of states is only about 3% less than ommlln2, the entropy of two maximally "entangled" elastic states. Note that for $\alpha = 0$ and $\alpha = 1$, the pure states 2 and 3 possess an entropy of "entanglement" of zero. The parameter α enables us to control the level of nonseparability of the superpositions of elastic states in a predictable manner.

3.2. Exploring the Hilbert space by tuning the relative driving phases

We have seen that the driving amplitude parameters have only a small effect on the relative phase between modes in the superposition of elastic states. In this subsection, we attempt to achieve more significant control on the relative phase between complex amplitudes in the Hilbert space of product states. For this, we are again using the external driving force $\vec{F}e^{i\omega_I t} = \left[(1-\alpha)E_{2'} + e^{i\phi_0}\gamma\alpha E_{3'}\right]e^{i\omega_I t}$ but with a nonzero phase ϕ_0 between the two spatial amplitudes $E_{2'}$ and $E_{3'}$. We use two output terminals of each of the three signal generators: one generator for each rod. We then drive the rods as follows:

$$\vec{F}\sin(\omega_I t) = \begin{pmatrix}F_1\\F_2\\F_3\end{pmatrix}\sin(\omega_I t) = \begin{pmatrix}(1-\alpha)\left|F_{FG_1CH_1}\right|\sin(\omega_I t) + \alpha\gamma\left|F_{FG_1CH_2}\right|\sin\left(\omega_I t + \Delta\phi_{FG_1} + \phi_0\right)\\(1-\alpha)\left|F_{FG_2CH_1}\right|\sin(\omega_I t) + \alpha\gamma\left|F_{FG_2CH_2}\right|\sin\left(\omega_I t + \Delta\phi_{FG_2} + \phi_0\right)\\(1-\alpha)\left|F_{FG_3CH_1}\right|\sin(\omega_I t) + \alpha\gamma\left|F_{FG_3CH_2}\right|\sin\left(\omega_I t + \Delta\phi_{FG_3} + \phi_0\right)\end{pmatrix} \tag{12}$$

where F_1, F_2, F_3 are the excitation amplitudes of rod 1, 2 and 3, respectively. In Eq. (12), the sub-script FG_i stands for ith function generator and CH_j stands for jth output channel of the generator, and hence $F_{FG_iCH_j}$ is the output voltage of channel CH_j of the FG_i signal generator. For the current study, we use: $\left|F_{FG_1CH_1}\right| = 1$, $\left|F_{FG_1CH_1}\right| = 0.1$, $\left|F_{FG_1CH_1}\right| = 1$, $\left|F_{FG_1CH_2}\right| = 1$, $\left|F_{FG_1CH_2}\right| = 2$, $\left|F_{FG_1CH_2}\right| = 1.4$; $\Delta\phi_{FG_1} = 0$, $\Delta\phi_{FG_2} = 0$, $\Delta\phi_{FG_3} = 180$, where $\Delta\phi_{FG_i} = \left\{\left(F_{FG_iCH_1} \times F_{FG_iCH_2}\right) < 0\right\} \times 180$ in degree; and ϕ_0 varies from 0 to 360 degree in steps of 10 degrees.

Again, in Fig. 2, we report the measured amplitude and phase characteristics of the elastic states in the space of rods (Fig. 2a,b) and the calculated amplitudes and phase of these states in the Hilbert space of superpositions of product states (Fig. 2c,d). Fig. 2 shows the dependency of these amplitudes and phases as a function of the driving phase ϕ_0. We again see that manipulation of the parameter ϕ_0 can be used to tune the eigen mode superposition characteristics in the space of the rods (see Figs. 2a and 2b). In the plots, the value of γ equals 1 and asterisks correspond to $\alpha = 0.25$, circles correspond to $\alpha = 0.50$, and squares correspond to $\alpha = 0.75$. Eq. (11) is again used to convert the representation of the elastic field from the space of the rods to the Hilbert space of superpositions of product states. Fig. 2c shows the variations of $|A_i|$ as functions of the driving parameter ϕ_0. In contrast with Fig. 1c, these moduli do not show drastic variations with ϕ_0 for fixed α and γ values, though they vary nonlinearly with ϕ_0. However, now the phase of the complex amplitudes and the phase difference between the E_2 and E_3 parts of the nonseparable superposition of states, $\left(\phi_{A_2} - \phi_{A_3}\right)$, varies significantly with ϕ_0 (see Fig. 2d). The driving phase parameter ϕ_0 provides a mean to significantly tune the phase of the complex amplitudes of nonseparable elastic states. Moreover, we note that the differences between the complex amplitude phase difference and input driving phase i.e., $\left(\left\{\phi_{A_2} - \phi_{A_3}\right\} + \phi_0\right)$ depends on α, regardless of input frequency values (see Figs. 3a and 3b). A larger α results in higher deviation of $\left(\left\{\phi_{A_2} - \phi_{A_3}\right\} + \phi_0\right)$ from the horizontal line (see Figs. 3a). Moreover, larger α's create higher magnitudes of both the rods amplitudes (see Fig. 2a) and the complex amplitudes (see Fig. 2c). This observation suggests that the output phase of the nonseparable states varies nonlinearly with the relative driving

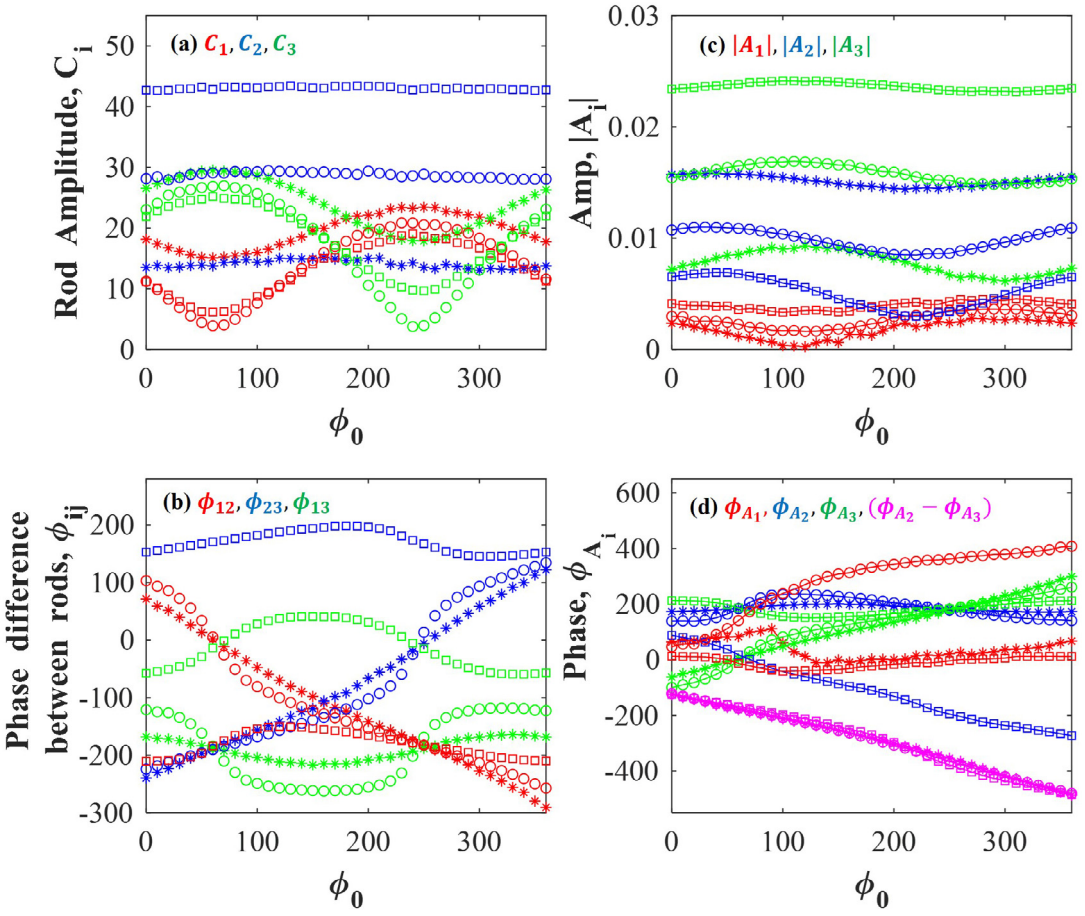

Fig. 2. Measured amplitude and phase characteristics of the elastic states in the space of rods (left panels) and calculated amplitudes and phase of states in the Hilbert space of superpositions of product states (right panels). Dependency on ϕ_0 of (**a**) the maximum amplitudes of each waveguide C_i, (**b**) the phase differences (ϕ_{ij}) between pairs of rods, (**c**) the modulus of the complex amplitudes $|A_i|$, and (**d**) the arguments ϕ_{A_i}. Here, $\gamma = 1$ and asterisks correspond to $\alpha = 0.25$, circles correspond to $\alpha = 0.50$, and squares correspond to $\alpha = 0.75$. The driving frequency $\omega_I = 48.8$ kHz. The amplitudes are in arbitrary units, the phases are in degrees, and ϕ_0 varies from 0 to 360 degrees.

amplitudes and phases applied to the waveguides. We hypothesize that deviations from the ideal model given by Eq. (1) are at the origin of such experimentally observed nonlinear behavior shown in Figs. 1–3. Let us focus again on the Bell state complex coefficients for the particular driving force $\vec{F} = (1-\alpha)\,E_{2'} + e^{i\phi_0}\gamma\alpha E_{3'}$:

$$A_i(k) = \frac{E_i.\left[(1-\alpha)\,E_{2'} + e^{i\phi_0}\gamma\alpha E_{3'}\right]}{\omega_{0,i}^2(k) - \omega_I^2 - i\eta\omega_I} = \frac{(1-\alpha)\,E_i.E_{2'} + e^{i\phi_0}\gamma\alpha E_i.E_{3'}}{\omega_{0,i}^2(k) - \omega_I^2 - i\eta\omega_I}. \tag{13}$$

Therefore, the Bell state coefficient $A_3(k)$ will be:

$$\begin{aligned} A_3(k) &= \gamma\alpha E_3.E_{3'}\frac{e^{i\phi_0}}{\omega_{0,3}^2(k) - \omega_I^2 - i\eta\omega_I} \\ &= \gamma\alpha E_3.E_{3'}e^{i\phi_0}\frac{\left[\left\{\omega_{0,3}^2(k) - \omega_I^2\right\} + i\eta\omega_I\right]}{\left\{\omega_{0,3}^2(k) - \omega_I^2\right\}^2 + (\eta\omega_I)^2} \\ &= \gamma\alpha E_3.E_{3'}e^{i\phi_0}\frac{\sqrt{\left\{\omega_{0,3}^2(k) - \omega_I^2\right\}^2 + (\eta\omega_I)^2}\,e^{i\left\{\tan^{-1}\left(\frac{\eta\omega_I}{\omega_{0,3}^2(k)-\omega_I^2}\right)\right\}}}{\left\{\omega_{0,3}^2(k) - \omega_I^2\right\}^2 + (\eta\omega_I)^2}, \end{aligned}$$

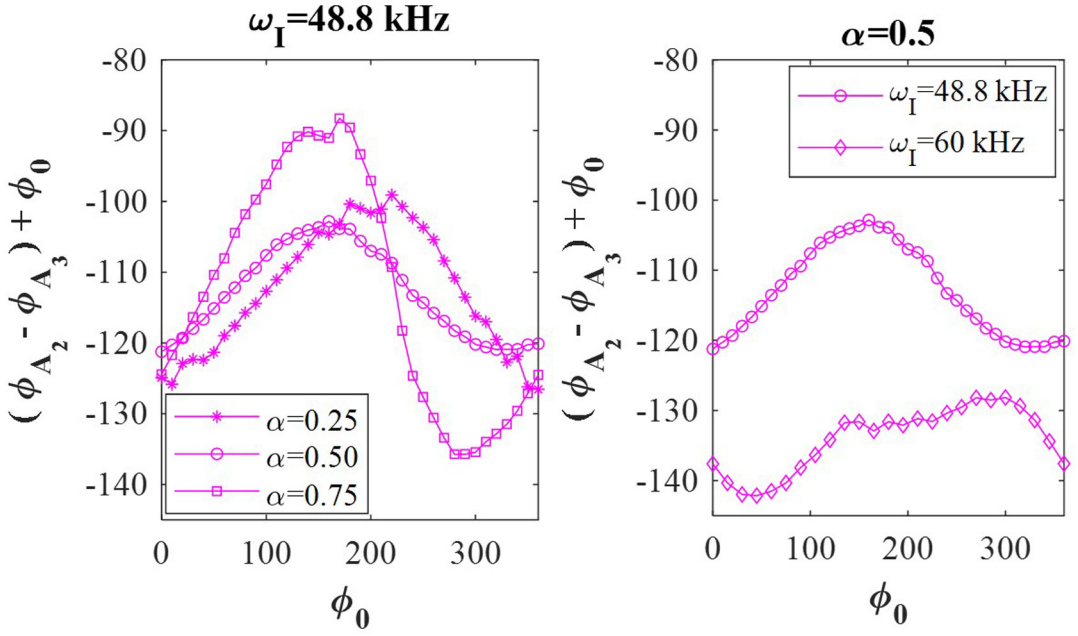

Fig. 3. Dependency on ϕ_0 of $\{(\phi_{A_2} - \phi_{A_3}) + \phi_0\}$. The phases are in degrees and ϕ_0 varies from 0 to 360 degrees. System parameter: $\gamma = 1$.

which leads to,

$$\phi_{A_3} = \phi_0 + \tan^{-1}\left(\frac{\eta\omega_I}{\omega_{0,3}^2(k) - \omega_I^2}\right).$$

Hence, we find:

$$\left(\{\phi_{A_2} - \phi_{A_3}\} + \phi_0\right) = \left[\tan^{-1}\left(\frac{\eta\omega_I}{\omega_{0,2}^2(k) - \omega_I^2}\right) - \tan^{-1}\left(\frac{\eta\omega_I}{\omega_{0,3}^2(k) - \omega_I^2}\right)\right]. \tag{14}$$

For fixed values of $\omega_{0,2}(k)$, $\omega_{0,3}(k)$ and ω_I, from Eq. (14) it is clear that for the case of (ideal) linearly coupled waveguides, the phase of the nonseparable states, $\phi_{A_2} - \phi_{A_3}$, should vary linearly with ϕ_0. This is true even in the presence of the complex amplitude $A_1(k)$, since it has no effect on Eq. (14). However, the deviations of the experimental results of Figs. 1–3 compared to the ideal system, unambiguously shows a dependency of the nonseparable states with the input driving amplitudes and phases. These differences suggest that additional phenomena, such as nonlinearity or irregularities, are at play in the experiment and need to be taken into account to improve the linear model (1). Hence, in the next section we develop a nonlinear numerical model based on discrete mass–spring waveguides. The model is used to study the complex behavior of nonseparable states in coupled waveguides. In particular, we are interested in identifying the physical parameters which lead to the unexpected nonlinear relationship between the phase difference between the complex amplitudes of a nonseparable superposition of elastic states and the driving phase.

Finally, we note in Fig. 3 that the experimentally measured phase differences $\{(\phi_{A_2} - \phi_{A_3}) + \phi_0\}$ versus ϕ_0 exhibit an overall oscillatory structure with a period of 360 degrees. These plots also show some finer features with possibly a shorter period.

4. Numerical modeling: Mass-spring waveguides

To numerically model the coupled waveguides, we assume that each rod constituting the experimental waveguide can be represented by a 1D crystal with harmonic approximation. Each rod consists of finite number of masses and springs with no pre-compression. The masses are constrained to move horizontal direction only. Therefore, the experimental coupled waveguides can be represented as a set of three 1D crystals with longitudinal harmonic springs coupled them along their length.

The experimental results of Section 3 illustrate that the coupled elastic waveguides does not comprise an ideal linear system. We have also observed that the relative phases and amplitudes of the nonseparable states vary nonlinearly with the relative driving amplitudes and phases applied to the waveguides. For this, we investigate the effect of nonlinearity in the elastic behavior of the medium coupling the waveguides. The coupling medium is constituted of epoxy, which

may exhibits some degree of nonlinearity in its elastic responses. In addition, inspection of the epoxy coupling between the aluminum rods shows some imperfections and irregularities along the direction of the rods. We therefore must also account for the possibility of a variation of the stiffness of the coupling along the rods. Hence, for a set of three coupled mass–spring chains with a total of N_m identical masses in each chain, the discrete elastic equations of motion are given by:

$$m\ddot{u}_n - k_{nn}\left(u_{n+1} - 2u_n + u_{n-1}\right) - k_{L,n}^{12}\left(v_n - u_n\right) - k_{NL}\left(v_n - u_n\right)^2 + \eta\dot{u}_n = 0, \tag{15a}$$

$$m\ddot{v}_n - k_{nn}\left(v_{n+1} - 2v_n + v_{n-1}\right) - k_{L,n}^{12}\left(u_n - v_n\right) - k_{L,n}^{23}\left(w_n - v_n\right) - k_{NL}\left(u_n - v_n\right)^2 - k_{NL}\left(w_n - v_n\right)^2 + \eta\dot{v}_n = 0, \tag{15b}$$

$$m\ddot{w}_n - k_{nn}\left(w_{n+1} - 2w_n + w_{n-1}\right) - k_{L,n}^{23}\left(v_n - w_n\right) - k_{NL}\left(v_n - w_n\right)^2 + \eta\dot{w}_n = 0. \tag{15c}$$

In Eq. (15), u_n, v_n and w_n are the displacements of nth mass of waveguides 1, 2, and 3, respectively. These quantities form the spatially discrete components of the 3×1 vector U_n for a continuous system. m denotes mass, η is the viscous damping coefficient that models the dissipation, and k_{nn} is the coupling constant of the nearest-neighbor interaction along a waveguide. k_L and k_{NL} describe the linear and nonlinear stiffness of the springs that couples the masses between the waveguides organized in a planar array. The effect of nonlinear behavior of the coupling medium is modeled by incorporating a quadratic nonlinearity, which is common in heterogeneous materials containing microcracks [47]. Imperfections and irregularities in the epoxy coupling are modeled by adding a randomly varying stiffness to the coupling along the waveguides. Hence, in Eq. (13), $k_{L,n}^{12}$ and $k_{L,n}^{23}$ describe the random linear stiffness of the springs that couples the masses between the waveguides (1,2) and (2,3), respectively. The specific values of the model Eq. (15) physical constants are $N_m = 48$, $\eta = 18.24$ Ns/m, $k_L = 33.5 \times 10^6$ N/m, $k_{NL} = 1.0 \times 10^6$ N/m, $k_{L,n}^{12} = k_L + 0.5\,\mathrm{rand}\,(N_m, 1)$, $k_{L,n}^{23} = k_L + 0.5\,\mathrm{rand}\,(N_m, 1)$ and $k_{L,n}^{12} \neq k_{L,n}^{23}$ (see Supplemental Material Note S3), where rand() function generates uniformly distributed random numbers between 0 and 1. Here, through the expression $k_L + 0.5\,\mathrm{rand}\,(N_m, 1)$ we have modeled the stiffness irregularities in the epoxy coupling between waveguides 1 and 2, and between waveguides 2 and 3.

To computationally generate the band structure, the Spectral Analysis of Amplitudes and Phases method [48] is employed, which we have recently developed and entails the use of molecular dynamics simulation. From the numerically obtained band structure plot (see Supplemental Material Note S3), we again identify two isofrequencies (48.1 kHz and 61.2 kHz) corresponding to (nearly) overlapping E_2 and E_3 modes. We can therefore use these frequencies to numerically realize a nonseparable superposition of states (including Bell states) and study the exploration of the corresponding Hilbert space. In the next subsections, we initially calibrate the model (Eq. (15)) by taking into account the nonlinear elastic behavior in the stiffness of the coupling, before combining nonlinearity and random variations in the stiffness in the last subsections.

4.1. Nonlinearly coupled waveguides

For the case of nonlinearly coupled mass–spring waveguides with no random variations in the stiffness of the coupling, we begin the numerical simulation by assuming $k_{L,n}^{12} = k_{L,n}^{23} = 0$.

4.1.1. Exploring the Hilbert space by tuning the relative driving amplitudes

In accord with the experiment, first we create a nonseparable state by exciting the coupled mass–spring waveguides at a frequency of 48.1 kHz with variable αandγ but with fixed ϕ_0. Fig. 4 shows the results for the amplitudes and phases presented in the same format as the experimental results. Fig. 4a shows the variations of the peak amplitudes of the last mass at the end of each waveguide C_i; $C_1 = \max\left(u_{N_m}(t)\right)$, $C_2 = \max\left(v_{N_m}(t)\right)$, $C_3 = \max\left(w_{N_m}(t)\right)$, and Fig. 4b shows the phase difference $\left(\phi_{ij}\right)$ between the displacements at the end of the waveguides for each pair of waveguides as functions of α, where $\phi_{12} = \frac{180}{\pi}\cos^{-1}\left(\frac{u_{N_m}(t).v_{N_m}(t)}{|u_{N_m}(t)||v_{N_m}(t)|}\right)$, $\phi_{23} = \frac{180}{\pi}\cos^{-1}\left(\frac{v_{N_m}(t).w_{N_m}(t)}{|v_{N_m}(t)||w_{N_m}(t)|}\right)$, $\phi_{13} = \frac{180}{\pi}\cos^{-1}\left(\frac{u_{N_m}(t).w_{N_m}(t)}{|u_{N_m}(t)||w_{N_m}(t)|}\right)$. From Figs. 4a and 4b we see that as is observed in the experimental results of Fig. 1, the parameter α can be used to numerically tune the eigen mode superposition. In the plots, asterisks correspond to $\gamma = 0.5$, circles correspond to $\gamma = 1.0$, and squares correspond to $\gamma = 2.5$. Using Eqs. (5) and (6), we determine the complex coefficients A_i, and report their respective modulus and phase in Figs. 4c and 4d. Due to the presence of weak nonlinearity, from Fig. 4c we observe weak nonlinear behavior of the coefficient A_i in the output response, as is observed in the experimental results of Fig. 1c. Moreover, the complex amplitudes are also a nonlinear function of γ, as is also observed in the experiment. Finally, from the inset of Fig. 4d we see that similarly to the experimental results of Fig. 1d, the phase of the nonseparable states $\left(\phi_{A_2} - \phi_{A_3}\right)$ depends only weakly on the driving amplitudes applied to the waveguides (α and γ). Hence, in accord with the experimental results of Fig. 1, Fig. 4 also demonstrates that for a fixed ϕ_0, tuning the driving amplitudes (α and γ) leads to significant variations in the modulus of the complex amplitudes of elastic superpositions of product states but does not effect significantly the phase of the nonseparable states. We therefore proceed to the next subsection to achieve more significant control on the phase of the nonseparable states by tuning ϕ_0.

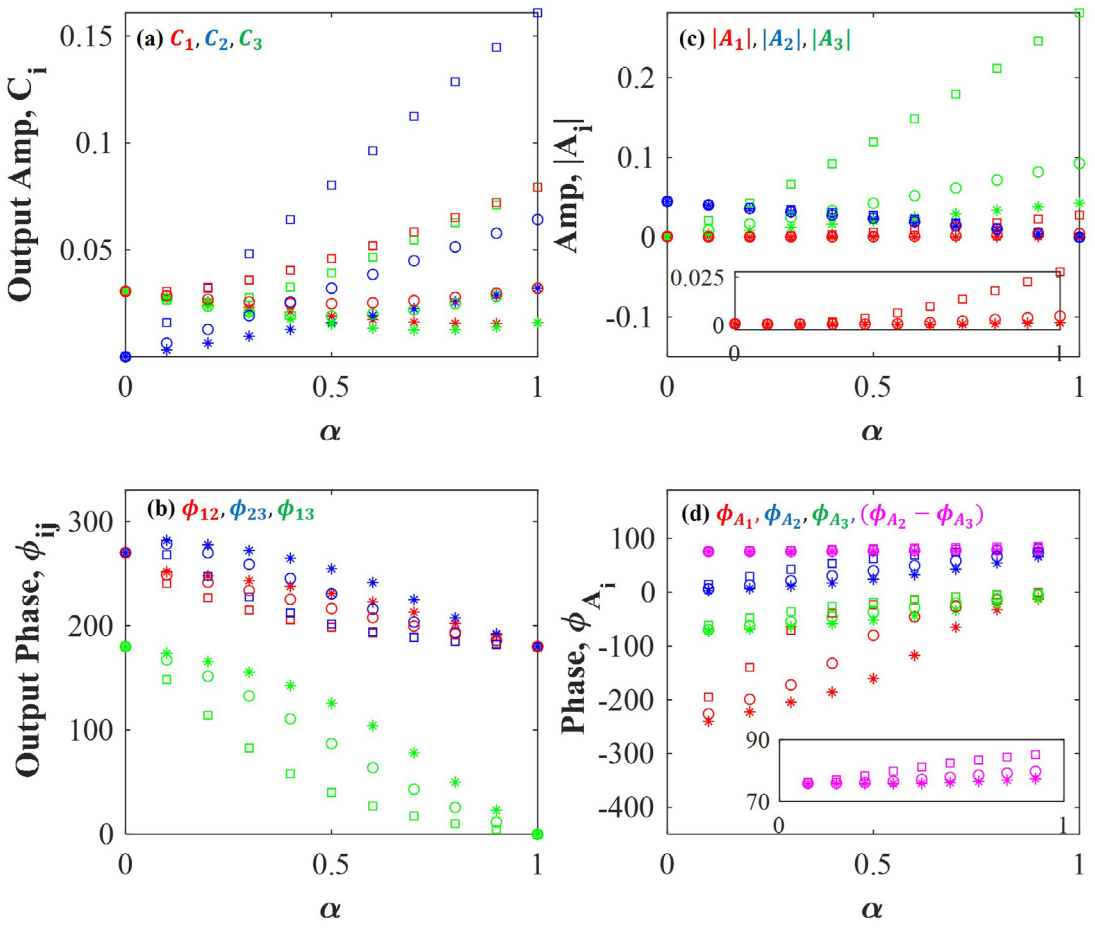

Fig. 4. Tuning of nonseparable states by the external driving force $\vec{F}e^{i\omega_l t}$; $\vec{F} = (1-\alpha)\,E_2 + e^{i\phi_0}\gamma\alpha E_3$, and driving frequency ω_l. Dependency on α of the (**a**) maximum amplitudes of the mass at the end of each waveguide C_i, (**b**) phase differences of displacement at the end of each waveguide (ϕ_{ij}) between pairs of chains, (**c**) modulus of the complex amplitudes $|A_i|$, and (**d**) arguments ϕ_{A_i}. In the plots, asterisks correspond to $\gamma = 0.5$, circles correspond to $\gamma = 1.0$, and squares correspond to $\gamma = 2.5$. The driving frequency $\omega_l = 48.1$ kHz. The amplitudes are in arbitrary units and the phases are in degrees.

4.1.2. Exploring the Hilbert space by tuning the relative driving phases

Fig. 5 shows the dependency of the coupled mass–spring waveguides when we tune the input phase of the nonseparable states ϕ_0. From Figs. 5a and 5b we again observe that manipulation of the parameter ϕ_0 can be used to numerically tune the eigen mode superposition (in agreement with Fig. 2). In all the plots, the value of γ equals 1 and asterisks correspond to $\alpha = 0.25$, circles correspond to $\alpha = 0.50$, and squares correspond to $\alpha = 0.75$. From Fig. 5c it is clear that due to the presence of weak nonlinearity, we see small variations of the complex coefficients $|A_i|$ with the input phase ϕ_0, as is also observed in the experimental results of Fig. 2c. On the other hand, for the case of (ideal) linearly coupled waveguide i.e., in the absence of nonlinearity, from Eq. (13) it is clear that the modulus of complex amplitudes $|A_i|$ has no effect on the variations of ϕ_0. However, due to the presence of nonlinearity, from Fig. 5d we observe that the quantity $\left(\{\phi_{A_2} - \phi_{A_3}\} + \phi_0\right)$ is not a horizontal line, and depends on α in a way reminiscent of the experimental results of Fig. 3. This clearly shows the need for nonlinearity in the numerical model since the linear model shown in Eq. (14) predicts only a linear relationship of $\{\phi_{A_2} - \phi_{A_3}\}$ with ϕ_0, and hence suggests that the experimental system includes nonlinearity.

The aforementioned findings suggest that the coupled elastic waveguides in our experiment functions as a nonlinear system. One thing to point out from Fig. 5 is that though the nonlinear model can fairly capture the experimental findings of Fig. 3, however the variations of $\left(\{\phi_{A_2} - \phi_{A_3}\} + \phi_0\right)$ with ϕ_0 is not well matched between the experimental system and the nonlinear numerical model (Figs. 3 and 5d). The experimental results exhibit oscillatory variations of $\left(\{\phi_{A_2} - \phi_{A_3}\} + \phi_0\right)$ with nearly a full period over the range of ϕ_0 (Fig. 3), whereas the nonlinear model shows almost two full period over the range of ϕ_0 (Fig. 5d). In addition, as mentioned above, inspection of the epoxy coupling between the aluminum rods shows some imperfections and irregularities along the direction of the rods. To account for these, in the next subsection we add random variations of the stiffness of the coupling along the waveguides of the numerical model to more closely match the variations of $\left(\{\phi_{A_2} - \phi_{A_3}\} + \phi_0\right)$ with ϕ_0 as is observed in the experiment.

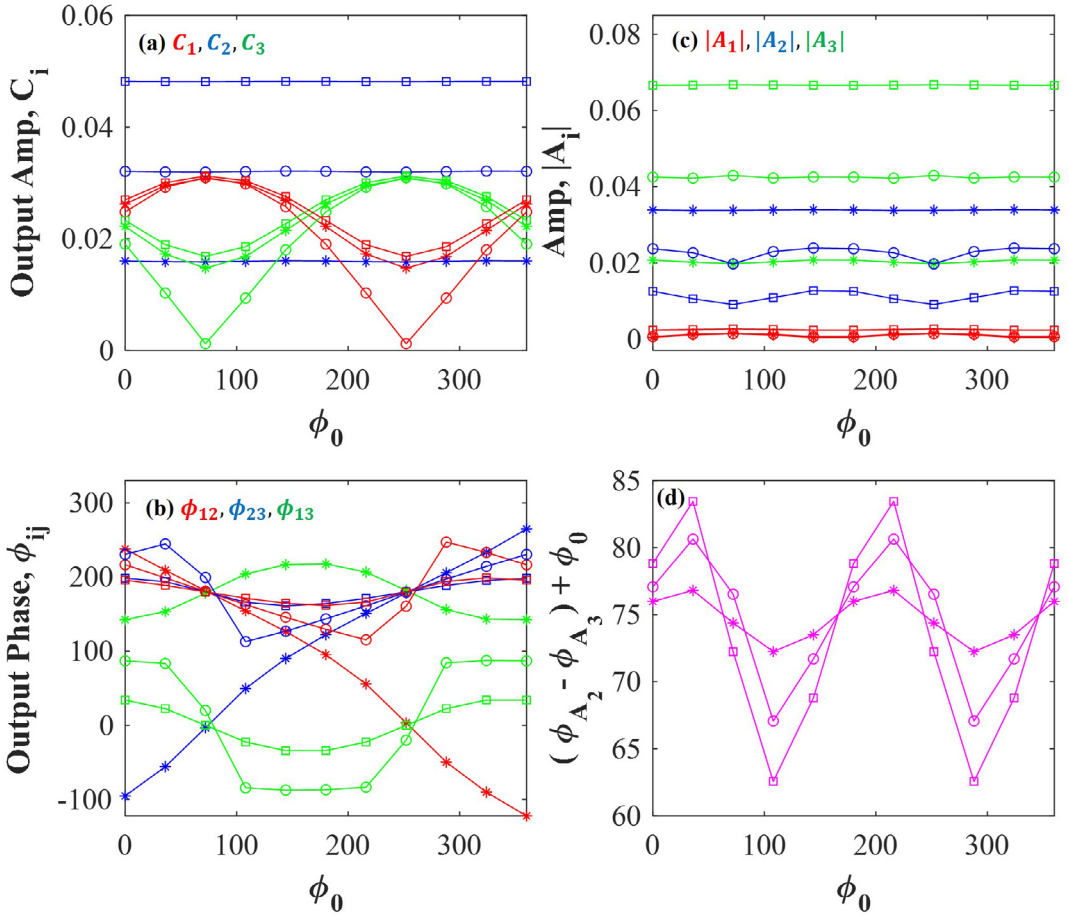

Fig. 5. Dependency on ϕ_0 of the (**a**) maximum amplitudes of the last mass of each waveguide C_i, (**b**) phase differences (ϕ_{ij}) between pairs of chains, (**c**) modulus of the complex amplitudes $|A_i|$, and (**d**) $(\{\phi_{A_2} - \phi_{A_3}\} - \phi_0)$. In the plots $\gamma = 1$ and asterisks correspond to $\alpha = 0.25$, circles correspond to $\alpha = 0.50$, and squares correspond to $\alpha = 0.75$. The driving frequency $\omega_l = 48.1$ kHz. The amplitudes are in arbitrary units and the phases are in degrees.

4.2. Nonlinearly coupled waveguides with random distribution of stiffness

We are now considering the combined effect of two of the phenomena, nonlinearity and randomness in the stiffness, which we believe may be playing a role in the observed experimental behavior. Fig. 6a shows the variations of $(\{\phi_{A_2} - \phi_{A_3}\} + \phi_0)$ with ϕ_0 for a particular sets of $k_{L,n}^{12}$ and $k_{L,n}^{23}$. By adding a uniform distribution of stiffness combined with nonlinearity, in Fig. 6a we observe a superposition feature: an almost single period in the variations of $(\{\phi_{A_2} - \phi_{A_3}\} + \phi_0)$ with ϕ_0 that matches well with the experimental result of Fig. 3. Nonlinearity of stiffness is crucial since as can be seen from Eq. (14) for the case of linearly coupled waveguides with no nonlinear stiffness of the coupling, the quantity $\{\phi_{A_2} - \phi_{A_3}\}$ should vary linearly with ϕ_0, which is however not the case for the experimental results (as shown in Figs. 1–3). Uniform distribution of stiffness, on the other hand, is needed to match the period of variations of phase of the nonseparable states with the input phase ϕ_0. Finally, we perform Fourier transform in space for the particular sets of $k_{L,n}^{12}$ and $k_{L,n}^{23}$ to reveal the wave numbers and hence the periodicity associated with the spatial pattern of the stiffness. From Figs. 6b and 6c we see that $k\,(2L) = 3$ and 13 has the highest amplitudes for the case of $k_{L,n}^{12}$, and $k\,(2L) = 5$ has the highest amplitudes for the case of $k_{L,n}^{23}$. The identification of few dominant wave numbers for the particular choices of $k_{L,n}^{12}$ and $k_{L,n}^{23}$ indicates that the coupling stiffness has some form of periodicity along their length and hence, we infer that the elastic waveguides are mutually coupled periodically. This suggests that both nonlinearity and periodicity in the coupling stiffness enables us to navigate a broad segment of the Hilbert space of product states.

5. Conclusion and discussion

Externally driven classical elastic waveguide systems, which are composed of parallel arrays of 1D aluminum rods coupled along their length with epoxy, are able to capture the characteristic of classical “entanglement” i.e., they can

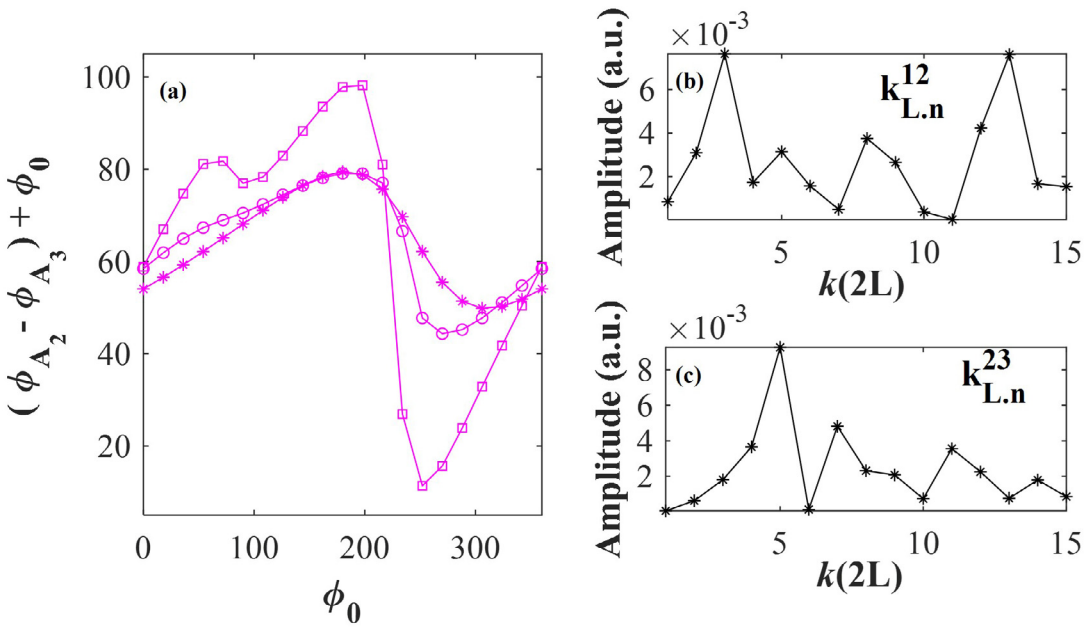

Fig. 6. (a) variations of $\left(\{\phi_{A_2} - \phi_{A_3}\} + \phi_0\right)$ with ϕ_0. In the plots $\gamma = 1$ and asterisks correspond to $\alpha = 0.25$, circles correspond to $\alpha = 0.50$, and squares correspond to $\alpha = 0.75$. (b) and (c) Spatial Fourier transform of the coupling stiffness $k^{12}_{L,n}$ and $k^{23}_{L,n}$ to reveal the wave numbers and hence the periodicity associated with the spatial pattern of the stiffness. The driving frequency $\omega_I = 48.1$ kHz. The amplitudes are in arbitrary units and the phases are in degrees.

support local nonseparable superpositions of product states. These nonseparable states, analogous to the Bell states, are the superposition of elastic waves, each a product of a plane wave part and spatial eigen modes. We have experimentally explored the different ways of manipulating the complex amplitude coefficients of these Bell states by driving these elastic systems externally. We have demonstrated that the frequency, relative amplitudes, and phases of the external drivers applied to the waveguides, are essential parameters for navigating the Hilbert space of these elastic product states. We have observed that the modulus of the complex amplitude of the nonseparable states can be significantly tuned by varying the relative amplitudes used to drive the waveguides. On the other hand, the phase of the drivers applied to the individual waveguides significantly affects the phase of the nonseparable states. Remarkably, our experimental results show that the phase difference between the complex amplitude coefficients of nonseparable states varies nonlinearly and significantly with the relative phase between the drivers. This unanticipated nonlinearity suggests that additional physical phenomena may be at play in the experiments. Therefore, we have developed a numerical model based on elastically coupled mass–spring waveguides, with the aim of shedding light on these possible phenomena. This model goes beyond linear elasticity and includes the nonlinear elasticity of the coupling medium between waveguides. It also incorporates randomly distributed variations in stiffness of the coupling medium along the waveguides to mimic possible experimental heterogeneities. Comparison between the experimental behavior and the numerical results confirms the importance of nonlinearity and inhomogeneities of the coupling stiffness. Adding a quadratic nonlinearity and randomly distributed heterogeneities in the stiffness of the coupling springs of the model, we were able to achieve qualitative agreement with the experimental findings. The model further shows that the presence of nonlinear elasticity and variations in stiffness of the coupling medium provide a means to extend the range of the elastic product states' Hilbert space that can be explored via external drivers. Nonlinear elasticity and heterogeneities in the medium coupling the waveguides can serve as parameters in the design of elastic systems which will enable the creation and manipulation of nonseparable states over a wide expanse of product states' Hilbert space. Expanding access to a broader range of the Hilbert space of elastic product states is essential for developing elasticity-based quantum analogue devices and quantum analogue information processing platforms since the Hilbert space dimension is the primary resource for quantum computation [49]. A quantum computer must have a Hilbert space whose dimension, in principle, is able to solve problems of arbitrary size. Moreover, navigation of the Hilbert space will eventually lead to the possibility of operating on the states, enabling the transformation of states analogous to quantum gates and, therefore, eventually developing algorithms.

CRediT authorship contribution statement

M. Arif Hasan: Conceived the idea of the research, Performed the theoretical studies, Fabricated the samples and built the experimental setups, Conducted the measurements, Analyzed the data, Scientific discussion and to writing the

manuscript. **Trevor Lata:** Fabricated the samples and built the experimental setups, Scientific discussion and to writing the manuscript. **Pierre Lucas:** Scientific discussion and to writing the manuscript. **Keith Runge:** Conceived the idea of the research, Performed the theoretical studies, Analyzed the data, Scientific discussion and to writing the manuscript. **Pierre A. Deymier:** Conceived the idea of the research, Performed the theoretical studies, Analyzed the data.

Declaration of competing interest

The authors declare that they have no known competing financial interests or personal relationships that could have appeared to influence the work reported in this paper.

Data availability

The data that support our findings of the present study are available from the corresponding author upon request.

Acknowledgments

We acknowledge financial support from the W.M. Keck Foundation. M.A.H. thanks Wayne State University Startup funds for support.

Appendix A. Supplementary data

Supplementary material related to this article can be found online at https://doi.org/10.1016/j.wavemoti.2022.102966.

References

[1] R. Horodecki, P. Horodecki, M. Horodecki, K. Horodecki, Quantum entanglement, Rev. Modern Phys. 81 (2) (2009) 865–942.
[2] E. Karimi, R.W. Boyd, Classical entanglement? Science 350 (6265) (2015) 1172–1173.
[3] R.J.C. Spreeuw, A classical analogy of entanglement, Found. Phys. 28 (3) (1998) 361–374.
[4] B.N. Simon, S. Simon, F. Gori, M. Santarsiero, R. Borghi, N. Mukunda, R. Simon, Nonquantum entanglement resolves a basic issue in polarization optics, Phys. Rev. Lett. 104 (2) (2010) 023901.
[5] P. Ghose, A. Mukherjee, Entanglement in classical optics, Rev. Theoret. Sci. 274 (2) (2014).
[6] E. Otte, I. Nape, C. Rosales-Guzmán, A. Vallés, C. Denz, A. Forbes, Recovery of nonseparability in self-healing vector bessel beams, Phys. Rev. A 98 (5) (2018) 053818.
[7] S.M. Hashemi Rafsanjani, M. Mirhosseini, O.S. Magaña-Loaiza, R.W. Boyd, State transfer based on classical nonseparability, Phys. Rev. A 92 (2) (2015) 023827.
[8] L.J. Pereira, A.Z. Khoury, K. Dechoum, Quantum and classical separability of spin-orbit laser modes, Phys. Rev. A 90 (5) (2014) 053842.
[9] M. McLaren, T. Konrad, A. Forbes, Measuring the nonseparability of vector vortex beams, Phys. Rev. A 92 (2) (2015) 023833.
[10] P.A. Deymier, K. Runge, Sound Topology, Duality, Coherence and Wave-Mixing: An Introduction to the Emerging New Science of Sound, Springer International Publishing, 2017.
[11] P.A. Deymier, K. Runge, Non-separable states in a bipartite elastic system, AIP Adv. 7 (4) (2017) 045020.
[12] M.A. Hasan, L. Calderin, T. Lata, P. Lucas, K. Runge, P.A. Deymier, The sound of bell states, Commun. Phys. 2 (1) (2019) 1–5.
[13] M.A. Hasan, L. Calderin, T. Lata, P. Lucas, K. Runge, P.A. Deymier, Directional elastic pseudospin and nonseparability of directional and spatial degrees of freedom in parallel arrays of coupled waveguides, Appl. Sci. 10 (9) (2020) 3202.
[14] M.A. Hasan, L. Calderin, T. Lata, P. Lucas, K. Runge, P.A. Deymier, Experimental demonstration of elastic analogues of nonseparable qutrits, Appl. Phys. Lett. 116 (16) (2020) 164104.
[15] B. Ndagano, B. Perez-Garcia, F.S. Roux, M. McLaren, C. Rosales-Guzman, Y. Zhang, O. Mouane, R.I. Hernandez-Aranda, T. Konrad, A. Forbes, Characterizing quantum channels with non-separable states of classical light, Nat. Phys. 13 (4) (2017) 397–402.
[16] S. Azzini, S. Mazzucchi, V. Moretti, D. Pastorello, L. Pavesi, Single-particle entanglement, Adv. Quantum Technol. 3 (10) (2020) 2000014.
[17] C. Schmid, A.P. Flitney, W. Wieczorek, N. Kiesel, H. Weinfurter, L.C.L. Hollenberg, Experimental implementation of a four-player quantum game, New J. Phys. 12 (6) (2010) 063031.
[18] A.R.C. Pinheiro, C.E.R. Souza, D.P. Caetano, J.A.O. Huguenin, A.G.M. Schmidt, A.Z. Khoury, Vector vortex implementation of a quantum game, J. Opt. Soc. Am. B, JOSAB 30 (12) (2013) 3210–3214.
[19] F. Töppel, A. Aiello, C. Marquardt, E. Giacobino, G. Leuchs, Classical entanglement in polarization metrology, New J. Phys. 16 (7) (2014) 073019.
[20] R. Jozsa, N. Linden, On the role of entanglement in quantum-computational speed-up, Proc. R. Soc. Lond. Ser. A Math. Phys. Eng. Sci. 459 (2036) (2003) 2011–2032.
[21] A. Aiello, F. Töppel, C. Marquardt, E. Giacobino, G. Leuchs, Quantum-like nonseparable structures in optical beams, New J. Phys. 17 (4) (2015) 043024.
[22] W.T. Buono, L.F.C. Moraes, J.A.O. Huguenin, C.E.R. Souza, A.Z. Khoury, Arbitrary orbital angular momentum addition in second harmonic generation, New J. Phys. 16 (9) (2014) 093041.
[23] C.E.R. Souza, J.A.O. Huguenin, P. Milman, A.Z. Khoury, Topological phase for spin-orbit transformations on a laser beam, Phys. Rev. Lett. 99 (16) (2007) 160401.
[24] L. Chen, W. She, Single-photon spin-orbit entanglement violating a bell-like inequality, J. Opt. Soc. Am. B, JOSAB 27 (6) (2010) A7–A10.
[25] C.V.S. Borges, M. Hor-Meyll, J.A.O. Huguenin, A.Z. Khoury, Bell-like inequality for the spin-orbit separability of a laser beam, Phys. Rev. A 82 (3) (2010) 033833.
[26] E. Karimi, J. Leach, S. Slussarenko, B. Piccirillo, L. Marrucci, L. Chen, W. She, S. Franke-Arnold, M.J. Padgett, E. Santamato, Spin-orbit hybrid entanglement of photons and quantum contextuality, Phys. Rev. A 82 (2) (2010) 022115.
[27] A. Vallés, V. D'Ambrosio, M. Hendrych, M. Mičuda, L. Marrucci, F. Sciarrino, J.P. Torres, Generation of tunable entanglement and violation of a bell-like inequality between different degrees of freedom of a single photon, Phys. Rev. A 90 (5) (2014) 052326.
[28] X.-F. Qian, B. Little, J.C. Howell, J.H. Eberly, Shifting the quantum-classical boundary: Theory and experiment for statistically classical optical fields, Optica 2 (7) (2015) 611–615.

[29] M. Michler, H. Weinfurter, M. Zukowski, Experiments towards falsification of noncontextual hidden variable theories, Phys. Rev. Lett. 84 (24) (2000) 5457–5461.
[30] B.R. Gadway, E.J. Galvez, F.D. Zela, Bell-inequality violations with single photons entangled in momentum and polarization, J. Phys. B: At. Mol. Opt. Phys. 42 (1) (2008) 015503.
[31] P.A. Deymier, K. Runge, Sound Topology, Duality, Coherence and Wave-Mixing: An Introduction to the Emerging New Science of Sound, Springer International Publishing, 2017.
[32] Y. Long, J. Ren, H. Chen, Intrinsic spin of elastic waves, Proc. Natl. Acad. Sci. USA 115 (40) (2018) 9951–9955.
[33] L. Calderin, M.A. Hasan, N.G. Jenkins, T. Lata, P. Lucas, K. Runge, P.A. Deymier, Experimental demonstration of coherent superpositions in an ultrasonic pseudospin, Sci. Rep. 9 (1) (2019) 1–10.
[34] B.-G. Englert, K.L. Lee, A. Mann, M. Revzen, Periodic and discrete zak bases, J. Phys. A: Math. Gen. 39 (7) (2006) 1669–1682.
[35] M.A. Hasan, L. Calderin, P. Lucas, K. Runge, P.A. Deymier, Geometric phase invariance in spatiotemporal modulated elastic system, J. Sound Vib. 459 (2019) 114843.
[36] H.-X. Wang, G.-Y. Guo, J.-H. Jiang, Band topology in classical waves: Wilson-Loop approach to topological numbers and fragile topology, New J. Phys. 21 (9) (2019) 093029.
[37] G. Brida, M.V. Chekhova, M. Genovese, L.A. Krivitsky, Two-photon entanglement generation: Different bell states within the linewidth of phase-matching, Opt. Express, OE 15 (16) (2007) 10182–10188.
[38] G. Brida, M. Chekhova, M. Genovese, L. Krivitsky, Generation of different bell states within the spontaneous parametric down-conversion phase-matching bandwidth, Phys. Rev. A 76 (5) (2007) 053807.
[39] S. Cialdi, F. Castelli, I. Boscolo, M.G. Paris, Generation of entangled photon pairs using small-coherence-time continuous wave pump lasers, Appl. Opt. AO 47 (11) (2008) 1832–1836.
[40] A.G. White, D.F.V. James, W.J. Munro, P.G. Kwiat, Exploring Hilbert space: Accurate characterization of quantum information, Phys. Rev. A 65 (1) (2001) 012301.
[41] P.G. Kwiat, E. Waks, A.G. White, I. Appelbaum, P.H. Eberhard, Ultrabright source of polarization-entangled photons, Phys. Rev. A 60 (2) (1999) R773–R776.
[42] S. Cialdi, F. Castelli, M.G.A. Paris, Properties of entangled photon pairs generated by a CW laser with small coherence time: Theory and experiment, J. Modern Opt. 56 (2–3) (2009) 215–225.
[43] P.A. Deymier, J.O. Vasseur, K. Runge, P. Lucas, Separability and nonseparability of elastic states in arrays of one-dimensional elastic waveguides, in: Phonons in Low Dimensional Structures, 2018.
[44] P.A. Deymier, K. Runge, J.O. Vasseur, A.-C. Hladky, P. Lucas, Elastic waves with correlated directional and orbital angular momentum degrees of freedom, J. Phys. B: At. Mol. Opt. Phys. 51 (13) (2018) 135301.
[45] P.A. Deymier, K. Runge, M.A. Hasan, L. Calderin, Exponentially complex 'classically entangled' states in arrays of one-dimensional nonlinear elastic waveguides, Materials 12 (21) (2019) 3553.
[46] D. Janzing, in: D. Greenberger, K. Hentschel, F. Weinert (Eds.), Entropy of Entanglement, Compendium of Quantum Physics, Springer, Berlin Heidelberg, Berlin, Heidelberg, 2009, pp. 205–209.
[47] K. Hoffmann, J.-Y. Kim, K. Scott, J. Qu, L.J. Jacobs, Excitation-dependent nonlinear behavior of distributed microcracks, AIP Conf. Proc. 2102 (1) (2019) 020039.
[48] M.A. Hasan, L. Calderin, P. Lucas, K. Runge, P.A. Deymier, Spectral analysis of amplitudes and phases of elastic waves: Application to topological elasticity, J. Acoust. Soc. Am. 146 (1) (2019) 748–766.
[49] R. Blume-Kohout, C.M. Caves, I.H. Deutsch, Climbing mount scalable: Physical resource requirements for a scalable quantum computer, Found. Phys. 32 (11) (2002) 1641–1670.